

Spatial-Spectral Feedback Network for Super-Resolution of Hyperspectral Imagery

Enhai Liu, Zhenjie Tang, Bin Pan, Zhenwei Shi

Abstract—Recently, single gray/RGB image super-resolution (SR) methods based on deep learning have achieved great success. However, there are two obstacles to limit technical development in the single hyperspectral image super-resolution. One is the high-dimensional and complex spectral patterns in hyperspectral image, which make it difficult to explore spatial information and spectral information among bands simultaneously. The other is that the number of available hyperspectral training samples is extremely small, which can easily lead to overfitting when training a deep neural network. To address these issues, in this paper, we propose a novel Spatial-Spectral Feedback Network (SSFN) to refine low-level representations among local spectral bands with high-level information from global spectral bands. It will not only alleviate the difficulty in feature extraction due to high dimensional of hyperspectral data, but also make the training process more stable. Specifically, we use hidden states in an RNN with finite unfoldings to achieve such feedback manner. To exploit the spatial and spectral prior, a Spatial-Spectral Feedback Block (SSFB) is designed to handle the feedback connections and generate powerful high-level representations. The proposed SSFN comes with a early predictions and can reconstruct the final high-resolution hyperspectral image step by step. Extensive experimental results on three benchmark datasets demonstrate that the proposed SSFN achieves superior performance in comparison with the state-of-the-art methods. The source code is available at <https://github.com/tangzhenjie/SSFN>.

Index Terms—Hyperspectral image, image super-resolution, deep convolutional neural networks, feedback mechanism.

I. INTRODUCTION

HYPERSPECTRAL imaging system collects and processes information across the entire range of electromagnetic spectrum. Compared with multispectral image or natural image, the resulting hyperspectral image (HSI) contains rich spectral information and have been widely used in various fields, such as plant detection [1], medical diagnosis [2], land cover detection [3], etc. However, due to the limitation of hardware, it is still difficult to acquire an HSI of high spatial resolution directly, which confines its practical applications.

This work was supported by the National Key R&D Program of China under the Grant 2019YFC1510900 and the National Natural Science Foundation of China under the Grant 62001251 and 62001252. (Corresponding author: Bin Pan.)

Enhai Liu and Zhenjie Tang are with the School of Artificial Intelligence, Hebei University of Technology, Tianjin 300401, China, and also with the Hebei Province Key Laboratory of Big Data Calculation, Tianjin 300401, China (e-mail: liuenhai@scse.hebut.edu.cn; tangzhenjie.hebut@gmail.com).

Bin Pan (Corresponding author) is with the School of Statistics and Data Science, Nankai University, Tianjin 300071, China (e-mail: pan-bin@nankai.edu.cn).

Zhenwei Shi is with the Image Processing Center, School of Astronautics, Beihang University, Beijing 100191, China (e-mail: shizhenwei@buaa.edu.cn).

Therefore, how to obtain a reliable high-resolution hyperspectral image remains a very challenging problem.

Image super-resolution (SR) is a promising signal post-processing technique, which aims at inferring a high-resolution image from one or sequential observed low-resolution images [4]. According to the number of input images, hyperspectral image super-resolution techniques can be divided into two categories: fusion-based hyperspectral image super-resolution and single hyperspectral image super-resolution [5]. The former improves the spatial resolution of the observed hyperspectral image by merging the observed low-resolution (LR) image with high-resolution (HR) auxiliary image (such as panchromatic, RGB, or multispectral image). For instance, Akhtar *et al.* [6] suggested using non-parametric Bayesian sparse representation to fuse a high-resolution RGB image with a low resolution hyperspectral image. By considering the hyperspectral image as a 3D tensor, Li *et al.* [7] proposed a coupled sparse tensor factorization fusion approach. Recently, deep learning-based fusion methods have achieved great success due to the powerful representational ability of convolution neural networks (CNNs) [8], [9]. Qi *et al.* [10] proposed a model-based deep learning approach for merging an high-resolution multispectral image and low-resolution hyperspectral images to generate a high-resolution hyperspectral image. Taking advantages of the powerful expression ability of CNNs, Wei *et al.* [11] explored a new HSI super-resolution network, which incorporates a deep structure as the regularizer/prior. However, most of these methods assume that the input auxiliary image is well co-registered with the low-resolution hyperspectral image. In practical applications, such well co-registered auxiliary images are usually hard or impossible to be accessed, which limits the progress of this type of method.

Compared with fusion-based hyperspectral image super-resolution, single hyperspectral image super-resolution has been limited advancement due complex spectral patterns in hyperspectral image and no auxiliary information. In order to explore the relationship between successive spectral bands, some single super-resolution approaches based on sparse and dictionary learning or low-rank approximation have been proposed [12], [13]. Huang *et al.* [12] proposed a novel super-resolution mapping method via multi-dictionary based sparse representation. Wang *et al.* [13] introduced a new tensor-based approach to solve the HSI super-resolution problem by modeling three three intrinsic characteristics of HSI. However, the hand-crafted priors can only reflect one aspect of the hyperspectral data.

Recently, the research of natural image super-resolution has achieved great success due to the use CNNs. Its main principle

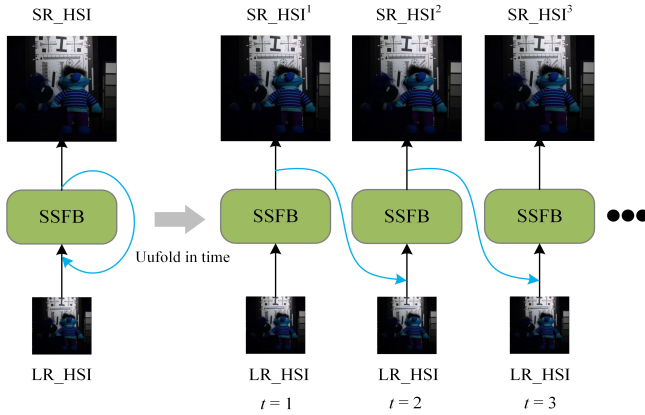


Fig. 1. The illustration of the feedback mechanism in the proposed network. Blue arrows represent the feedback connections. Spatial-Spectral Feedback Block (SSFB) receives the information of input and hidden state from last iteration, then passes its hidden state to next iteration.

is to learn a mapping function from low-resolution to high-resolution in a supervised way. The typical networks include SRCNN [14], EDSR [15], and SRGAN [16], etc. Compared with natural image super-resolution based on deep learning, in the single hyperspectral image super-resolution task, there are two difficulties that hinder its further development: on the one hand, due to high-dimensional and complex spectral patterns in hyperspectral data, it is hard to explore the spatial information and the spectral information between bands simultaneously. On the other hand, hyperspectral images are not as popular as natural images, the number of available training samples is extremely small. Even if we can collect a lot of hyperspectral images, the obtained images may be from different hyperspectral cameras. The differences in the number of spectral bands and imaging conditions will make it difficult to establish a unified deep network. Furthermore, it is easy to cause the over-fitting problem. To handle these problems, Jiang *et al.* [17] recently introduced a spatial-spectral network (SSPN) to exploit spatial information and the correlation between the spectral bands. They implemented a group convolution (with shared network parameters) and progressive upsampling framework to stabilize the training process. However, they did not deeply investigate the spectral correlation among groups, which limited the network’s ability to extract spectral feature.

In order to deal with the above problems, in this paper, we proposed a novel network for single hyperspectral super-resolution, namely Spatial-Spectral Feedback Network (SSFN). Motivated by the feedback mechanism [18], the proposed SSFN can refine low-level representations among local spectral bands using high-level information from global spectral bands through feedback connections. The SSFN is essentially an RNN with a Spatial-Spectral Feedback Block (SSFB), which is specifically designed to explore the spatial and spectral prior for hyperspectral image super-resolution task. The SSFB is constructed by local and global spectral feature extraction layer to generate powerful high-level global spectral representation. Inspired by [19], we use the output of the SSFB (i.e., a hidden state in an unfold RNN) to achieve

the feedback manner. Specifically, the hidden state at each iteration flows into the next iteration to modulate the local spectral low-level representation input. In order to ensure the hidden state contains the information of the high-resolution hyperspectral image, we connect the loss to each iteration during the training process. The principle of the feedback scheme is that the information of a coarse SR hyperspectral image can facilitate an LR hyperspectral image to reconstruct a better SR hyperspectral image (as the Fig. 1 shows).

In summary, our contributions are as follows:

- A novel Spatial-Spectral Feedback Network (SSFN) is proposed for the single hyperspectral image super-resolution.
- A feedback mechanism is designed to provide the global spectral high-level information in top-down feedback flows through feedback connections. In addition, such recurrent architecture with feedback connections needs only few parameters that alleviate the overfitting issue in a single hyperspectral image super-resolution task.
- A Spatial-Spectral Feedback Block (SSFB) is proposed to fully explore the spatial-spectral prior of hyperspectral images, which refine the local spectral low-level representation using the global spectral high-level information through feedback connections.

II. RELATED WORK

In this section, we briefly review some approaches that are most relevant to our work, which include fusion-based hyperspectral image super-resolution, single hyperspectral image super-resolution and feedback mechanism.

A. Fusion-based Hyperspectral Image Super-Resolution

Recently, the spatial resolution enhancement technique focused on low-resolution hyperspectral image and high-resolution multispectral image fusion has received extensive attention. For example, Yokoya *et al.* [20] designed a coupled nonnegative matrix factorization (CNMF) based approach to improve the spatial resolution of hyperspectral image. Based on the spatial-spectral sparsity of hyperspectral image, Dong *et al.* [21] proposed a sparse representation approach to estimate the hyperspectral dictionary and the sparse codes for enhancing the spatial resolution. Some methods have also been proposed to exploit redundancy and correlation in the spectral domain by exploiting non-local similarity [22], self-similarity [23], multiple structure clustering [24], low-rank constraints [25]. Most recently, some deep learning based methods have become popular due to its excellent performance [26]–[28]. The principle of the above fusion-based hyperspectral image super-resolution methods is to borrow the high-frequency spatial information from high-resolution auxiliary image and fuse this information to generate the target high-resolution hyperspectral image. Through these approaches have achieved very good performance, the co-registered auxiliary image with high-resolution is very arduous, which limit the progress of practical application.

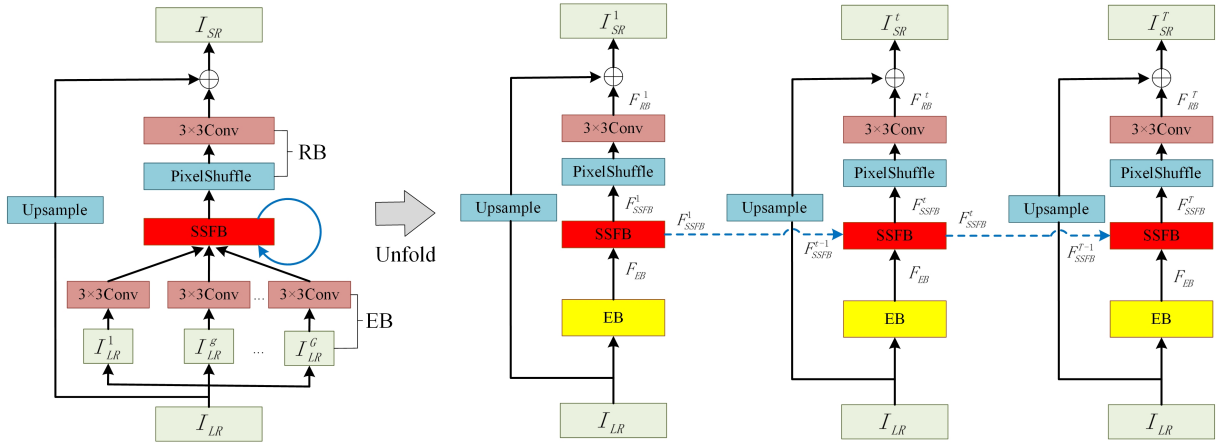


Fig. 2. The overview of our proposed Spatial-Spectral Feedback Network (SSFN). The blue arrows represent feedback connections.

B. Single Hyperspectral Image Super-Resolution

Compared with fusion-based hyperspectral image super-resolution approaches, single hyperspectral image super-resolution does not need co-registered auxiliary image, which has better feasibility in practice. Akgun *et al.* [4] proposed a pioneer work, in which a hyperspectral image acquisition model and the projection onto convex sets (POCS) algorithm is adopted to reconstruct the high-resolution hyperspectral image. By incorporating the low-rank and group-sparse in-prior knowledge, Huang *et al.* [29] designed a novel method to deal with the unknown blurring problem. Recently, some researchers also studied sparse representations and dictionary learning based approaches [13], [30]. However, there are some drawbacks to these methods. Firstly, in the testing process, they typically need to solve complex and time-consuming optimization problems. Secondly, these handcrafted priors only reflect one aspect of the hyperspectral data. Due to the great success of deep neural network in computer vision [31], deep learning techniques have also recently been introduced to the single hyperspectral super-resolution task. For instance, Xie *et al.* [32] firstly adopted CNNs to super-resolve the hyperspectral image and then use the nonnegative matrix factorization (NMF) to guarantee the spectral characteristic for the intermediate results. Mei *et al.* [33] showed that a 3D CNN can be utilized for the hyperspectral image super-resolution and achieved excellent performance. Although the spectral correlation can be well exploited by 3D convolution, the computational complexity is very large. In order to reduce the amount of calculation, Li *et al.* [34] proposed a grouped deep recursive residual network (GDRRN) by designing a recursive group module and integrating it into a residual structure. Jiang *et al.* [17] also recently proposed a spatial-spectral prior network (SSPN) to fully exploit the spatial information and the correlation between the spectral bands. They designed a group convolution (with shared network parameters) and progressive upsampling framework to stabilize the training process. In general, compared with traditional methods, these deep learning based methods achieve better results. However, due to the limited hyperspectral images and high dimensionality of spectral bands, it is difficult to

explore spatial information and spectral information among bands simultaneously.

C. Feedback Mechanism

In cognition theory, feedback connections linking cortical visual areas can transmit response signals from higher-order areas to lower-order areas [35]. Motivated by this phenomenon, recent studies have adopted this feedback mechanism to design the network architecture for various vision tasks [19], [36]–[40]. The feedback mechanism in these network architectures allows the high-level information back to previous layers and refines low-level encoded information.

As for image SR, some researchers have also made efforts to introduce a feedback mechanism. For example, Haris *et al.* [38] designed up- and down-projection units to provide an error feedback mechanism. Based on delayed feedback, Han *et al.* [39] proposed a dual-state RNN, in which information between two recurrent states are exchanged in both directions. However, the flow of information to generate the final SR image is still feedforward in their network architectures, making it impossible for previous layers to access useful information from the following layers. The most relevant work to ours is [40], which refines low-level representations with high-level information using feedback connections in an RNN. However, it aims at solving natural image super-resolution task. To fit a feedback mechanism in hyperspectral image super-resolution, we elaborately design a Spatial-Spectral Feedback Block as the basic module in our SSFN. Experimental results indicate that the Spatial-Spectral Feedback Block is more suitable for hyperspectral image SR tasks.

III. THE PROPOSED SSFN METHOD

A. Network Architecture

As shown in Fig. 2, our proposed SSFN can be unfolded to T iterations, where each iteration t is ordered from 1 to T . Similar to [40], in order to make the hidden state in SSFN carry a notion of output, we tie the loss for every iteration. The detailed description of the loss function can be found in the next Loss Function part. The sub-network

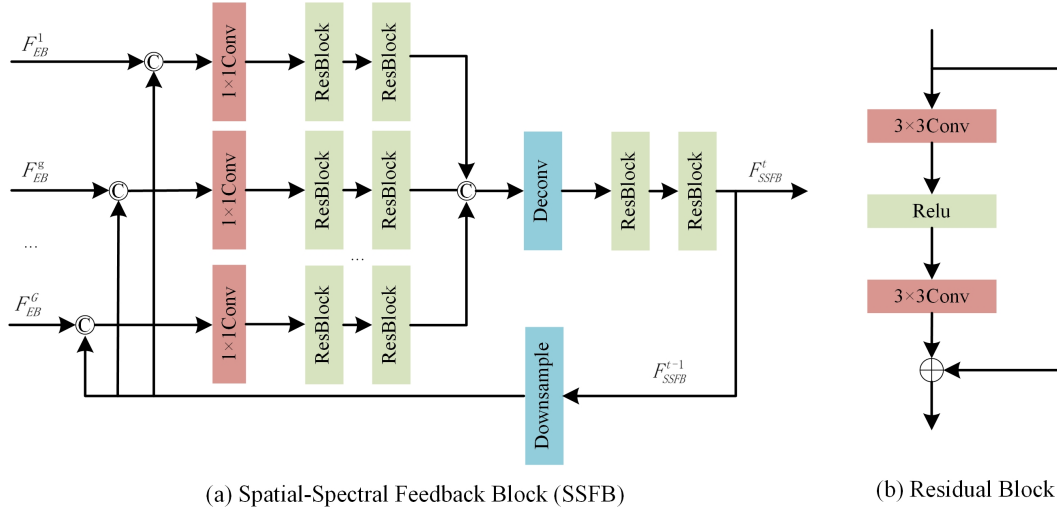


Fig. 3. The network architecture of the Spatial-Spectral Feedback Block (SSFB): (a) the Spatial-Spectral Feedback Block, (b) the Residual Block

in each iteration t consists of three parts: the Embedding Block (EB), the Spatial-Spectral Feedback Block (SSFB) and the Reconstruction Block (RB). The weights of each block are shared across time. The global residual skip connection at each iteration t delivers an up-sampled image to bypass the sub-network. Therefore, the purpose of the sub-network at each iteration t is to recover a residual image, while input a low-resolution hyperspectral image.

1) *The Embedding Block*: Different from previous methods, which treat the hyperspectral image as a whole or multiple single channel images, we divide the whole hyperspectral image into several groups. In this way, we can not only explore the correlations among neighboring spectral bands of the input hyperspectral image, but also reduce the spectral dimensionality of each group. Specifically, the input low-resolution hyperspectral image I_{LR} is firstly divided into G groups, $I_{LR} = \{I_{LR}^1, I_{LR}^2, \dots, I_{LR}^G\}$. More details are discussed in the experiment section. As shown in Fig. 2, for each group I_{LR}^g , we directly apply one convolution operation to extract its shallow feature F_{EB}^g as in [41],

$$F_{EB} = f_{EB}(I_{LR}) \quad (1)$$

where the f_{EB} denotes the operations of Embedding Block, eg., feature extraction layer for all groups. $F_{EB} = \{F_{EB}^1, F_{EB}^2, \dots, F_{EB}^G\}$ is then used as input to the Spatial-Spectral Feedback Block.

2) *The Spatial-Spectral Feedback Block*: Spatial-spectral feedback block at t -th iteration receives the hidden state from previous iteration F_{SSFB}^{t-1} through a feedback connection and the shallow feature F_{EB}^t . F_{SSFB}^t denotes the output of SSFB. The mathematical formulation of the SSFB is as follows:

$$F_{SSFB}^t = f_{SSFB}(F_{SSFB}^{t-1}, F_{EB}^t) \quad (2)$$

where f_{SSFB} represents the operations of the SSFB. More details of the SSFB can be found in Spatial-Spectral Feedback Block section.

3) *The Reconstruction Block*: The reconstruction block uses PixelShuffle [42] to upscale the feature F_{SSFB}^t to HR one and a convolution operation to generate a residual image I_{Res}^t . The mathematical formulation of the reconstruction block is:

$$I_{Res}^t = f_{RB}(F_{SSFB}^t) \quad (3)$$

where f_{RB} denotes the operations of the reconstruction block.

The output image I_{SR}^t at t -th iteration can be obtained by:

$$I_{SR}^t = I_{Res}^t + f_{UP}(I_{LR}) \quad (4)$$

Where f_{UP} denotes the operation of an upsample kernel. The choice of the upsample kernel is arbitrary. In this paper, we use a Bicubic upsample kernel. After T iterations, we will get T SR images $(I_{SR}^1, I_{SR}^2, \dots, I_{SR}^T)$.

B. Spatial-Spectral Feedback Block

Image super-resolution is a ill-posed problem, which calls for additional prior (regulation) to constrain the reconstruction process. Traditional approaches try to design sophisticated regulation terms such as low-rank [43], total variation [44] and sparse [6] by hand. Therefore, the performance of the super-resolution methods is heavily dependent on whether the designed prior can well characterize the observed data. For the hyperspectral image super-resolution, it is very important to study the inherent characteristics of hyperspectral images, e.g., the spatial non-local self-similarity and the high-correlation between spectra. The manually designed constraints are not enough to achieve accurate restoration of hyperspectral images.

In this paper, we design a Spatial-Spectral Feedback Block to exploit the spatial and spectral prior. As shown in Fig. 3, the SSFB at the t -th iteration receives the feedback global spectral high-level information F_{SSFB}^{t-1} to correct the G groups local spectral low-level representations, $F_{EB} = \{F_{EB}^1, F_{EB}^2, \dots, F_{EB}^G\}$, and then generates more powerful high-level representations F_{SSFB}^t for the next iteration and the reconstruction block. The SSFB contains G groups local spectral feature

extraction layers and one global spectral feature extraction layer. We denote $Conv(k)$ and $Deconv(k)$ as a convolution layer and a deconvolutional layer respectively, where k is the size of the filter.

At the beginning of the SSFB, the downsampled F_{SSFB}^{t-1} and each group F_{EB}^g are concatenated and compressed by one $Conv(1)$ operation to refine the input each group feature F_{EB}^g by feedback information F_{SSFB}^{t-1} , producing the refined group feature F_g^t .

$$F_g^t = f_{Com}([f_{Down}(F_{SSFB}^{t-1}), F_{EB}^g]) \quad (5)$$

where f_{Down} refers to downsample operation using average pooling with a kernel of 2 and stride of 2. The $[f_{Down}(F_{SSFB}^{t-1}), F_{EB}^g]$ refers to the concatenation of $f_{Down}(F_{SSFB}^{t-1})$ and F_{EB}^g . The f_{Com} denotes the initial compression operation.

After obtaining the refined group feature F_g^t , we add a local spectral feature extraction layer to explore the local spectral correlation, which consists of two residual blocks as shown in Fig. 3(b). Let L_g^t be the g -th group local spectral LR feature map. L_g^t can be obtained by:

$$L_g^t = f_{Local}(F_g^t) \quad (6)$$

where the f_{Local} denotes local spectral feature extraction layer.

After that, we pass all the local spectral LR feature maps to the global spectral feature extraction layer, which contains one upsample $Deconv(2)$ operation and two residual blocks. Note that we propose a strategy of progressive super-resolution reconstruction to stabilize the training process. Particularly, in addition to the reconstruction block, we also add an upsampling operation in the global spectral feature extraction layer. At last, the global spectral high-level feature F_{SSFB}^t can be obtained by:

$$F_{SSFB}^t = f_{Global}([L_1^t, L_2^t, \dots, L_G^t]) \quad (7)$$

where the f_{Global} denotes the the global spectral feature extraction layer.

C. Loss Function

In order to measure the super-resolution performance, we choose $L1$ loss to optimize our proposed network. A target high-resolution hyperspectral image I_{HR} is placed to fit in the multiple output in our proposed network. The final output is the average of all intermediate predictions:

$$I_{SR} = \frac{1}{T} \sum_{t=1}^T I_{Res}^t + f_{UP}(I_{LR}) \quad (8)$$

The loss function in the network can be formulated as:

$$L(\Theta) = \|I_{HR} - I_{SR}\|_1 \quad (9)$$

where the Θ denotes to the parameters of our network.

IV. EXPERIMENTS AND RESULTS

A. Datasets

1) *CAVE dataset*: The CAVE dataset is collected by a cooled CCD camera at a 10 nm step from 400nm to 700nm (31 bands) [45]. The dataset contains 32 scenes, split into five sections: food and drinks, skin and hair, paints, real and fake, and stuff. The size of the hyperspectral images is $512 \times 512 \times 31$ in this dataset.

2) *Harvard dataset*: The Harvard dataset is captured by a commercial hyperspectral camera (Nuance FX, CRI Inc) in the wavelength range of 400 nm to 700 nm [46]. The dataset consists of 77 hyperspectral images from real-world indoor and outdoor scenes. The size of all the hyperspectral images is $1040 \times 1392 \times 31$ in this dataset.

3) *Foster dataset*: The Foster dataset is taken by a low-noise Peltier-cooled digital camera [47]. The dataset includes 30 hyperspectral images acquired from the Minho region of Portugal during late spring and summer of 2002 and 2003. Each hyperspectral image has 33 spectral bands and 1204×1344 pixels in total.

B. Implementation Details

Compared with the natural image SR, we need to train and test each dataset individually because different datasets are collected by different hyperspectral cameras. In our experiments, 80% of the samples are randomly selected as training set and the remaining samples are used for testing.

During the training phase, we randomly choose 12 patches and put them to the SSFN network. According to the scale factor s , these patches are downsampled as low-resolution hyperspectral image with the size of $32 \times 32 \times L$ by the bicubic interpolation. The L is the number of spectral bands. In our work, in order to ensure that the size of the feature map is not changed, the zero-padding strategy is applied for these Conv layers with kernel size 3×3 . We use the deconvolution with a kernel 2 and a stride 2 to upsample the feature map by a factor 2. The ADAM [48] with an initial learning rate of $2e-4$ is used to optimize the SSFN network.

In the test phase, in order to improve the test efficiency, we only use the top left 512×512 region of each test image for evaluation. We use Pytorch libraries to implement and train our proposed SSFN network.

C. Evaluation Metrics

To comprehensively evaluate the performance of our proposed method, six quantitative measurements (PQIs) are utilized: cross correlation (CC) [51], spectral angle mapper (SAM) [52], root mean squared error (RMSE), the erreur relative globale adimensionnelle de synthese (ERGAS) [53], peak signal-to-noise ratio (PSNR) and structure similarity (SSIM) [54]. CC, RMSE, PSNR and SSIM are widely used quantitative metrics for image quality assessment, and their detailed descriptions are omitted in this paper. ERGAS is a

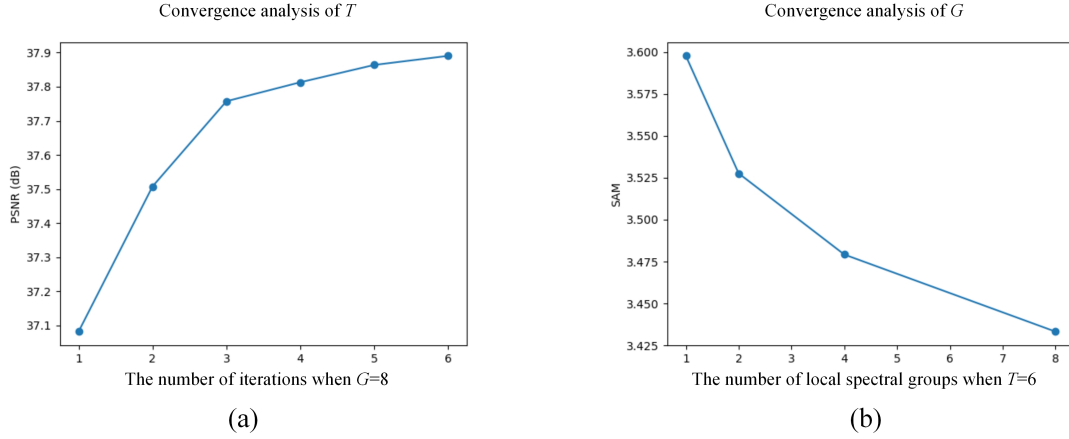
Fig. 4. Convergence analysis of T and G on CAVE with scaling factor $\times 4$.

TABLE I
AVERAGE QUANTITATIVE COMPARISONS OF SEVEN DIFFERENT APPROACHES OVER TESTING IMAGES FROM CAVE DATASET WITH RESPECT TO SIX PQIS.

	s	CC \uparrow	SAM \downarrow	RMSE \downarrow	ERGAS \downarrow	PSNR \uparrow	SSIM \uparrow
Bicubic	4	0.9846	5.1832	0.0224	7.7384	34.5069	0.9472
VDSR [49]	4	0.9896	4.3622	0.0188	6.3067	36.1348	0.9612
RCAN [50]	4	0.9913	4.3058	0.0172	5.7796	36.7979	0.9657
3DCNN [33]	4	0.9862	4.2297	0.0212	7.3182	34.9853	0.9549
GDRRN [34]	4	0.9891	4.2970	0.0192	6.5087	35.8465	0.9594
SSPSR [17]	4	<u>0.9915</u>	<u>3.7384</u>	<u>0.0168</u>	<u>5.7527</u>	<u>37.0479</u>	<u>0.9682</u>
SSFN	4	0.9930	3.4332	0.0152	5.1599	37.8905	0.9737
Bicubic	8	0.9564	7.3210	0.0385	12.8323	29.5763	0.8741
VDSR [49]	8	0.9615	5.8692	0.0369	12.0527	30.0080	0.8999
RCAN [50]	8	0.9671	5.9008	<u>0.0340</u>	11.1373	30.7372	0.9061
3DCNN [33]	8	0.9594	<u>5.6079</u>	0.0370	12.3341	29.8880	0.8961
GDRRN [34]	8	0.9611	5.8864	0.0368	12.0684	30.0042	0.8966
SSPSR [17]	8	<u>0.9675</u>	5.6617	0.0341	<u>11.0506</u>	<u>30.7976</u>	<u>0.9098</u>
SSFN	8	0.9712	5.0550	0.0323	10.3982	31.4007	0.9159

TABLE II
AVERAGE QUANTITATIVE COMPARISONS OF SEVEN DIFFERENT APPROACHES OVER TESTING IMAGES FROM HARVARD DATASET WITH RESPECT TO SIX PQIS.

	s	CC \uparrow	SAM \downarrow	RMSE \downarrow	ERGAS \downarrow	PSNR \uparrow	SSIM \uparrow
Bicubic	4	0.9606	2.5671	0.0101	3.0957	43.9037	0.9582
VDSR [49]	4	0.9640	2.5709	0.0090	2.8602	44.6486	0.9634
RCAN [50]	4	0.9671	2.4097	0.0086	2.7537	45.1204	0.9663
3DCNN [33]	4	0.9614	2.3917	0.0098	3.0324	44.1815	0.9600
GDRRN [34]	4	0.9630	2.4924	0.0093	2.9276	44.4577	0.9620
SSPSR [17]	4	<u>0.9704</u>	<u>2.2766</u>	<u>0.0082</u>	<u>2.5893</u>	<u>45.5460</u>	<u>0.9684</u>
SSFN	4	0.9722	2.2496	0.0074	2.4463	46.1866	0.9730
Bicubic	8	0.9098	3.0165	0.0179	5.0694	39.6681	0.9131
VDSR [49]	8	0.9185	3.0093	0.0165	4.7369	40.2490	0.9223
RCAN [50]	8	0.9312	2.7808	0.0150	4.3438	40.9853	<u>0.9313</u>
3DCNN [33]	8	0.9128	2.7853	0.0172	4.9422	39.9615	0.9175
GDRRN [34]	8	0.9175	2.8669	0.0166	4.7946	40.1831	0.9214
SSPSR [17]	8	<u>0.9338</u>	2.6202	<u>0.0149</u>	<u>4.2458</u>	<u>41.1869</u>	<u>0.9313</u>
SSFN	8	0.9373	<u>2.7665</u>	0.0139	4.0316	41.6320	0.9374

global statistical measure of the SR quality, which is calculated by

$$ERGAS(I_{HR}, I_{SR}) = 100s \sqrt{\frac{1}{L} \sum_{l=1}^L \left(\frac{RMSE_l}{\mu_l} \right)^2} \quad (10)$$

in which $RMSE_l = (\|I_{SR}^l - I_{HR}^l\|_F / \sqrt{n})$. Here, n denotes the number of pixel in any band of I_{HR} and μ_l is the sample mean of the l th band of ground truth I_{HR} . The I_{SR}^l and I_{HR}^l denote the l th band of I_{SR} and I_{HR} , respectively. The SAM is utilized to evaluate the spectral information preservation at each pixel. The SAM is defined as the spectral angle between the reconstructed spectra $\hat{\mathbf{x}}$ and its corresponding ground truth spectra \mathbf{x} , which is defined as

$$SAM(\mathbf{x}, \hat{\mathbf{x}}) = \arccos \left(\frac{\langle \mathbf{x}, \hat{\mathbf{x}} \rangle}{\|\mathbf{x}\|_2 \|\hat{\mathbf{x}}\|_2} \right) \quad (11)$$

in which $\langle \cdot, \cdot \rangle$ denotes dot product of two vectors and $\|\mathbf{x}\|_2$ is the l_2 norm of a vector. For PSNR and SSIM, we report their mean values of all spectral bands. The best values for

CC, SAM, RMSE, ERGAS, PSNR, SSIM are 1, 0, 0, 0, $+\infty$, and 1, respectively.

D. Study of T and G

In this section, we explored the influence of the number of iterations (denoted as T) and the number of local spectral groups in the Spatial-Spectral Feedback Block (denoted as G). In subsequent experiments, we set the base number of filters to 256. We first explore the influence of T by fixing G to 8. It can be seen from Fig. 4(a) that compared with the network without feedback connections ($T=1$), the reconstruction performance is significantly improved with the help of feedback connections. Moreover, with the increase of the iterations T , the quality of reconstruction has been further improved. In other words, our proposed Spatial-Spectral Feedback Block surely benefits from the feedback information across time. After that, we study the influence of G by fixing the T to 6. From Fig. 4(b), we observe that with the help of local-spectral grouping strategy, the spectral reconstruction performance is greatly improved

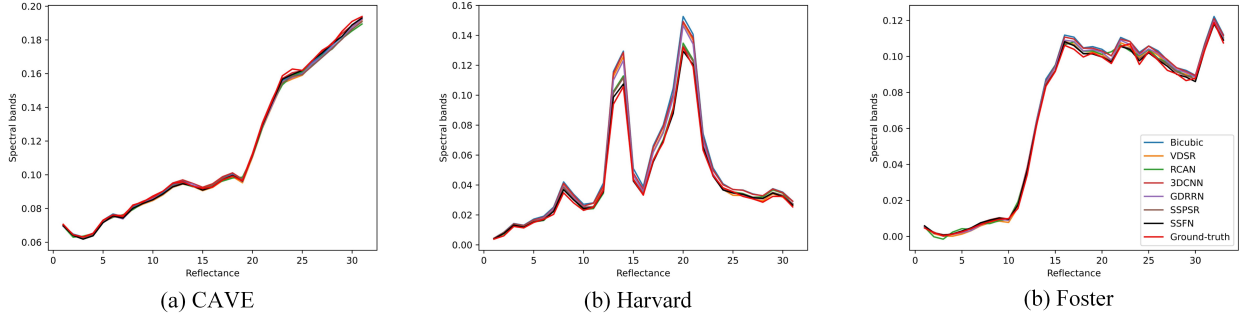


Fig. 5. Visual comparisons of spectral distortion for image *paints* on CAVE dataset, image *imgh0* on Harvard dataset and image *Tibaes_Garden* on Foster dataset. The curves are the average results of spectral curves in pixel position (20, 20), (100, 100), and (340, 340).

TABLE III
AVERAGE QUANTITATIVE COMPARISONS OF SEVEN DIFFERENT APPROACHES OVER TESTING IMAGES FROM FOSTER DATASET WITH RESPECT TO SIX PQIS.

	s	CC \uparrow	SAM \downarrow	RMSE \downarrow	ERGAS \downarrow	PSNR \uparrow	SSIM \uparrow
Bicubic	4	0.9751	7.8624	0.0066	4.5223	47.3676	0.9772
VDSR [49]	4	0.9766	7.5076	0.0058	4.3478	48.1376	0.9810
RCAN [50]	4	0.9769	7.4178	0.0057	4.7053	47.9460	0.9815
3DCNN [33]	4	0.9765	7.7497	0.0063	4.4313	47.6749	0.9793
GDRRN [34]	4	0.9770	7.3068	0.0058	4.3137	48.0862	0.9811
SSPSR [17]	4	<u>0.9799</u>	<u>6.7713</u>	<u>0.0054</u>	<u>4.0099</u>	<u>48.7576</u>	<u>0.9834</u>
SSFN	4	0.9818	6.6966	0.0051	3.8070	49.2753	0.9851
Bicubic	8	0.9175	11.2534	0.0149	8.8529	40.6677	0.9169
VDSR [49]	8	0.9203	10.0831	0.0142	8.7204	40.9915	0.9299
RCAN [50]	8	0.9206	9.7229	0.0142	9.0382	40.9188	0.9299
3DCNN [33]	8	0.9224	10.5045	0.0148	8.7102	40.8497	0.9282
GDRRN [34]	8	0.9206	9.8813	0.0144	8.7659	40.8964	0.9292
SSPSR [17]	8	<u>0.9268</u>	8.9278	0.0135	<u>8.3273</u>	<u>41.4176</u>	<u>0.9352</u>
SSFN	8	0.9280	<u>9.0651</u>	<u>0.0136</u>	8.2217	41.4414	0.9363

compared with the network without the grouping strategy ($G=1$). In addition, when the G continues to increase, the spectral reconstruction quality keeps rising due to the stronger spectral representative ability. In conclusion, choosing larger T or G can obtain better super-resolution results. In the following experiments, we set $T=6$, $G=8$ for analysis.

E. Comparisons with the State-of-the-Art Methods

In this section, we present a detailed evaluation of our approach on three public hyperspectral image datasets, *i.e.*, CAVE dataset [45], Harvard dataset [46] and Foster dataset [47]. We compare the proposed method with five existing SR methods, including two state-of-the-art deep single gray/RGB image super-resolution methods, VDSR [49], RCAN [50], and three representative deep single hyperspectral image super-resolution methods, 3DCNN [33], GDRRN [34] and SSPSR [17]. In order to obtain the best performance, we carefully adjust the hyperparameters of these comparison methods. The bicubic interpolation is used as our baseline. Table I, II and III depict the average objective performance over testing images of all comparison algorithms on three datasets, where bold denotes the best result, underline represents the second best.

As shown in Table I, our proposed SSFN method significantly outperforms other algorithms with respect to all objective evaluation indexes. Specifically, the Bicubic produces the worst performance among these comparison algorithms. As the most competitive general gray/RGB image super-resolution methods, VDSR and RCAN can produce quite pleasurable results. However, their SAM indices are relatively poor when compared with those single hyperspectral image super-resolution approaches, *i.e.*, 3DCNN [33] and SSPSR [17]. Similar to our proposed method, SSPSR [17] also adopts a group strategy, which can well explore the spectral information. Thus, it achieves the second best results for the SAM indices. Compared with the existing SR methods, our method can obtain better performance. In the term of PSNR, the proposed method for upsampling factor $d = 4/8$ are 0.8 and 0.6 higher than the second best method, respectively. The similar results can also be found in Table II and III, except for SAM. In summary, the SSFN achieves good performance in comparison to existing SR methods on three dataset, particularly in PSNR and SSIM.

In Fig. 6, 7 and 8, we show the visual comparison results with different algorithms for scale factor $\times 4$ on three datasets. These figures only depict the visual results of the 27-th band of three typical scenes. In order to observe the difference between the reconstructed hyperspectral image and ground-truth clearly, we present the absolute error map between them. Generally, the bluer the absolute error map is, the better the reconstructed image is. From these figures, we can easily observe that our proposed SSFN method can obtain the lower absolute error results.

Moreover, we also visualize the spectral distortion of the reconstructed images. We draw spectral curves for three scenes in Fig. 5. To alleviate the problem caused by random selection, we first select the spectra of three pixel positions ((20, 20), (100, 100), and (340, 340)), and then calculate the average result of the three spectral curves. As shown in Fig. 5, the spectral curves of all comparison methods are basically consistent with the ground-truth. However, curves of our proposed method SSFN are much closer to the ground-truth in most cases, which proves that our approach has better spectral reconstruction ability.

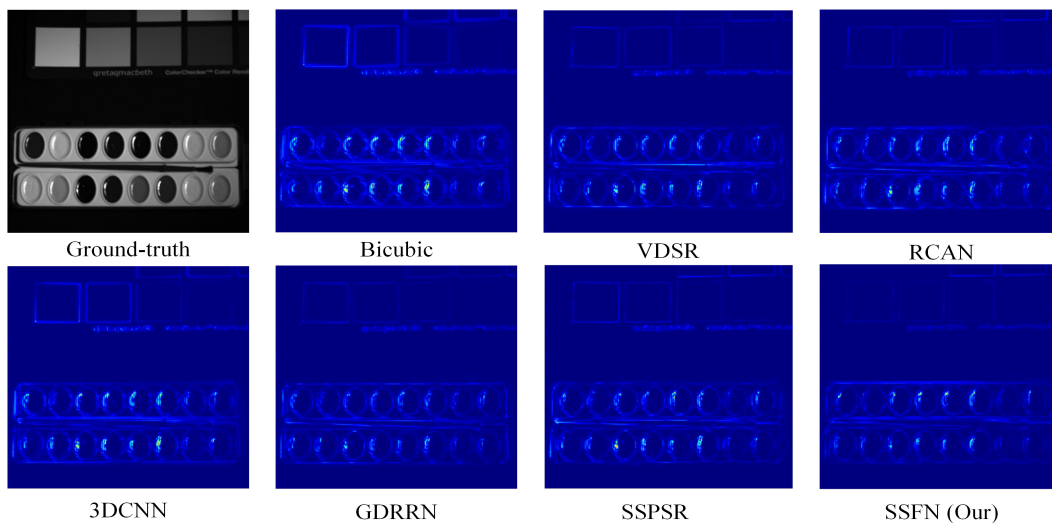


Fig. 6. Absolute error map comparisons for image *paints* on CAVE dataset.

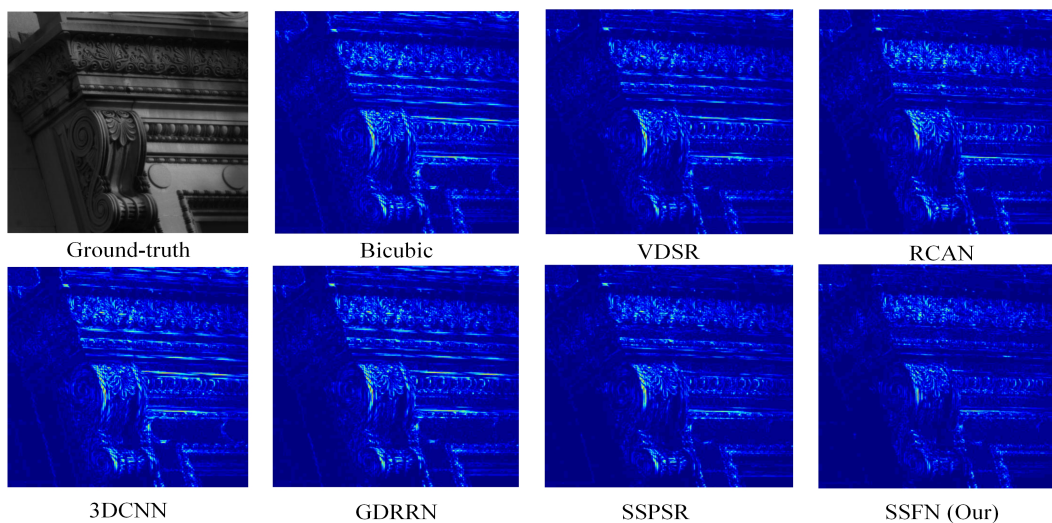


Fig. 7. Absolute error map comparisons for image *img0* on Harvard dataset.

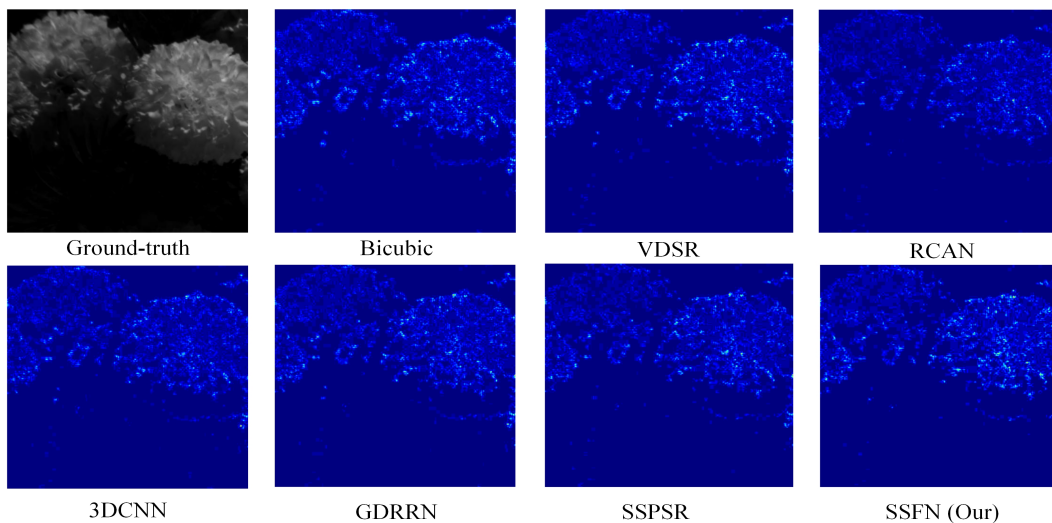


Fig. 8. Absolute error map comparisons for image *Tibaes_Garden* on Foster dataset.

V. CONCLUSION

In this paper, we propose a novel network for single hyperspectral image super-resolution called Spatial-Spectral Feedback Network (SSFN), which can faithfully reconstruct a SR hyperspectral image by enhancing low-level local-spectral representations with the high-level global-spectral ones. In particular, in order to explore the spatial and spectral correlation characteristic of hyperspectral data, we carefully designed a Spatial-Spectral Feedback Block (SSFB) to handle the feedback information flow as well as the feature reuse. In addition, such recurrent structure with feedback connections requires only few parameters, which makes it possible to obtain stable training results under small data. The comprehensive experimental results on three public hyperspectral datasets have demonstrated that the proposed SSFN not only achieves the best performance in terms of some commonly used objective indicators, but also generates more clear high-resolution images in comparison with the state-of-the-art methods.

REFERENCES

- [1] A. Lowe, N. Harrison, and A. P. French, "Hyperspectral image analysis techniques for the detection and classification of the early onset of plant disease and stress," *Plant methods*, vol. 13, no. 1, pp. 1–12, 2017.
- [2] R. Pike, G. Lu, D. Wang, Z. G. Chen, and B. Fei, "A minimum spanning forest-based method for noninvasive cancer detection with hyperspectral imaging," *IEEE Transactions on Biomedical Engineering*, vol. 63, no. 3, pp. 653–663, 2015.
- [3] K. Liu, H. Su, and X. Li, "Estimating high-resolution urban surface temperature using a hyperspectral thermal mixing (htm) approach," *IEEE Journal of Selected Topics in Applied Earth Observations and Remote Sensing*, vol. 9, no. 2, pp. 804–815, 2015.
- [4] T. Akgun, Y. Altunbasak, and R. M. Mersereau, "Super-resolution reconstruction of hyperspectral images," *IEEE Transactions on Image Processing*, vol. 14, no. 11, pp. 1860–1875, 2005.
- [5] N. Yokoya, C. Grohnfeldt, and J. Chanussot, "Hyperspectral and multispectral data fusion: A comparative review of the recent literature," *IEEE Geoscience and Remote Sensing Magazine*, vol. 5, no. 2, pp. 29–56, 2017.
- [6] N. Akhtar, F. Shafait, and A. Mian, "Bayesian sparse representation for hyperspectral image super resolution," in *2015 IEEE Conference on Computer Vision and Pattern Recognition (CVPR)*, 2015, pp. 3631–3640.
- [7] S. Li, R. Dian, L. Fang, and J. M. Bioucas-Dias, "Fusing hyperspectral and multispectral images via coupled sparse tensor factorization," *IEEE Transactions on Image Processing*, vol. 27, no. 8, pp. 4118–4130, 2018.
- [8] Y. Chang, L. Yan, H. Fang, S. Zhong, and W. Liao, "Hsi-denet: Hyperspectral image restoration via convolutional neural network," *IEEE Transactions on Geoscience and Remote Sensing*, vol. 57, no. 2, pp. 667–682, 2019.
- [9] O. Sidorov and J. Yngve Hardeberg, "Deep hyperspectral prior: Single-image denoising, inpainting, super-resolution," in *Proceedings of the IEEE/CVF International Conference on Computer Vision Workshops*, 2019, pp. 0–0.
- [10] Q. Xie, M. Zhou, Q. Zhao, D. Meng, W. Zuo, and Z. Xu, "Multispectral and hyperspectral image fusion by ms/hs fusion net," in *Proceedings of the IEEE/CVF Conference on Computer Vision and Pattern Recognition*, 2019, pp. 1585–1594.
- [11] W. Wei, J. Nie, Y. Li, L. Zhang, and Y. Zhang, "Deep recursive network for hyperspectral image super-resolution," *IEEE Transactions on Computational Imaging*, vol. 6, pp. 1233–1244, 2020.
- [12] H. Huang, J. Yu, and W. Sun, "Super-resolution mapping via multi-dictionary based sparse representation," in *2014 IEEE International Conference on Acoustics, Speech and Signal Processing (ICASSP)*, 2014, pp. 3523–3527.
- [13] W. Yao, C. Xia, H. Zhi, and H. Shiyang, "Hyperspectral image super-resolution via nonlocal low-rank tensor approximation and total variation regularization," *Remote Sensing*, vol. 9, no. 12, p. 1286, 2017.
- [14] C. Dong, C. C. Loy, K. He, and X. Tang, "Learning a deep convolutional network for image super-resolution," in *European conference on computer vision*. Springer, 2014, pp. 184–199.
- [15] B. Lim, S. Son, H. Kim, S. Nah, and K. Mu Lee, "Enhanced deep residual networks for single image super-resolution," in *Proceedings of the IEEE conference on computer vision and pattern recognition workshops*, 2017, pp. 136–144.
- [16] C. Ledig, L. Theis, F. Huszar, J. Caballero, A. Cunningham, A. Acosta, A. Aitken, A. Tejani, J. Totz, Z. Wang, *et al.*, "Photo-realistic single image super-resolution using a generative adversarial network," in *Proceedings of the IEEE conference on computer vision and pattern recognition*, 2017, pp. 4681–4690.
- [17] J. Jiang, H. Sun, X. Liu, and J. Ma, "Learning spatial-spectral prior for super-resolution of hyperspectral imagery," *IEEE Transactions on Computational Imaging*, vol. 6, pp. 1082–1096, 2020.
- [18] J. Hupé, A. James, B. Payne, S. Lomber, P. Girard, and J. Bullier, "Cortical feedback improves discrimination between figure and background by v1, v2 and v3 neurons," *Nature*, vol. 394, no. 6695, pp. 784–787, 1998.
- [19] A. R. Zamir, T.-L. Wu, L. Sun, W. B. Shen, B. E. Shi, J. Malik, and S. Savarese, "Feedback networks," in *Proceedings of the IEEE conference on computer vision and pattern recognition*, 2017, pp. 1308–1317.
- [20] N. Yokoya, T. Yairi, and A. Iwasaki, "Coupled nonnegative matrix factorization unmixing for hyperspectral and multispectral data fusion," *IEEE Transactions on Geoscience and Remote Sensing*, vol. 50, no. 2, pp. 528–537, 2011.
- [21] W. Dong, F. Fu, G. Shi, X. Cao, J. Wu, G. Li, and X. Li, "Hyperspectral image super-resolution via non-negative structured sparse representation," *IEEE Transactions on Image Processing*, vol. 25, no. 5, pp. 2337–2352, 2016.
- [22] Y. Xu, Z. Wu, J. Chanussot, and Z. Wei, "Nonlocal patch tensor sparse representation for hyperspectral image super-resolution," *IEEE Transactions on Image Processing*, vol. 28, no. 6, pp. 3034–3047, 2019.
- [23] X.-H. Han, B. Shi, and Y. Zheng, "Self-similarity constrained sparse representation for hyperspectral image super-resolution," *IEEE Transactions on Image Processing*, vol. 27, no. 11, pp. 5625–5637, 2018.
- [24] L. Zhang, W. Wei, C. Bai, Y. Gao, and Y. Zhang, "Exploiting clustering manifold structure for hyperspectral imagery super-resolution," *IEEE Transactions on Image Processing*, vol. 27, no. 12, pp. 5969–5982, 2018.
- [25] M. A. Veganzones, M. Simoes, G. Licciardi, N. Yokoya, J. M. Bioucas-Dias, and J. Chanussot, "Hyperspectral super-resolution of locally low rank images from complementary multisource data," *IEEE Transactions on Image Processing*, vol. 25, no. 1, pp. 274–288, 2015.
- [26] J. Yang, X. Fu, Y. Hu, Y. Huang, X. Ding, and J. Paisley, "Pannet: A deep network architecture for pan-sharpening," in *Proceedings of the IEEE international conference on computer vision*, 2017, pp. 5449–5457.
- [27] R. Dian, S. Li, A. Guo, and L. Fang, "Deep hyperspectral image sharpening," *IEEE transactions on neural networks and learning systems*, vol. 29, no. 11, pp. 5345–5355, 2018.
- [28] R. A. Borsoi, T. Imbiriba, and J. C. M. Bermudez, "Super-resolution for hyperspectral and multispectral image fusion accounting for seasonal spectral variability," *IEEE transactions on image processing*, vol. 29, pp. 116–127, 2019.
- [29] H. Huang, J. Yu, and W. Sun, "Super-resolution mapping via multi-dictionary based sparse representation," in *2014 IEEE International Conference on Acoustics, Speech and Signal Processing (ICASSP)*. IEEE, 2014, pp. 3523–3527.
- [30] J. Li, Q. Yuan, H. Shen, X. Meng, and L. Zhang, "Hyperspectral image super-resolution by spectral mixture analysis and spatial-spectral group sparsity," *IEEE Geoscience and Remote Sensing Letters*, vol. 13, no. 9, pp. 1250–1254, 2016.
- [31] W. Yang, X. Zhang, Y. Tian, W. Wang, J.-H. Xue, and Q. Liao, "Deep learning for single image super-resolution: A brief review," *IEEE Transactions on Multimedia*, vol. 21, no. 12, pp. 3106–3121, 2019.
- [32] W. Xie, X. Jia, Y. Li, and J. Lei, "Hyperspectral image super-resolution using deep feature matrix factorization," *IEEE Transactions on Geoscience and Remote Sensing*, vol. 57, no. 8, pp. 6055–6067, 2019.
- [33] S. Mei, X. Yuan, J. Ji, Y. Zhang, S. Wan, and Q. Du, "Hyperspectral image spatial super-resolution via 3d full convolutional neural network," *Remote Sensing*, vol. 9, no. 11, p. 1139, 2017.
- [34] Y. Li, L. Zhang, C. Ding, W. Wei, and Y. Zhang, "Single hyperspectral image super-resolution with grouped deep recursive residual network," in *2018 IEEE Fourth International Conference on Multimedia Big Data (BigMM)*. IEEE, 2018, pp. 1–4.
- [35] C. D. Gilbert and M. Sigman, "Brain states: top-down influences in sensory processing," *Neuron*, vol. 54, no. 5, pp. 677–696, 2007.
- [36] C. Cao, X. Liu, Y. Yang, Y. Yu, J. Wang, Z. Wang, Y. Huang, L. Wang, C. Huang, W. Xu, *et al.*, "Look and think twice: Capturing top-down visual attention with feedback convolutional neural networks," in

- Proceedings of the IEEE international conference on computer vision*, 2015, pp. 2956–2964.
- [37] J. Carreira, P. Agrawal, K. Fragkiadaki, and J. Malik, “Human pose estimation with iterative error feedback,” in *Proceedings of the IEEE conference on computer vision and pattern recognition*, 2016, pp. 4733–4742.
- [38] M. Haris, G. Shakhnarovich, and N. Ukita, “Deep back-projection networks for super-resolution,” in *Proceedings of the IEEE conference on computer vision and pattern recognition*, 2018, pp. 1664–1673.
- [39] W. Han, S. Chang, D. Liu, M. Yu, M. Witbrock, and T. S. Huang, “Image super-resolution via dual-state recurrent networks,” in *Proceedings of the IEEE conference on computer vision and pattern recognition*, 2018, pp. 1654–1663.
- [40] Z. Li, J. Yang, Z. Liu, X. Yang, G. Jeon, and W. Wu, “Feedback network for image super-resolution,” in *Proceedings of the IEEE/CVF Conference on Computer Vision and Pattern Recognition*, 2019, pp. 3867–3876.
- [41] J. Li, Y. Yuan, K. Mei, and F. Fang, “Lightweight and accurate recursive fractal network for image super-resolution,” in *Proceedings of the IEEE/CVF International Conference on Computer Vision Workshops*, 2019, pp. 0–0.
- [42] W. Shi, J. Caballero, F. Huszár, J. Totz, A. P. Aitken, R. Bishop, D. Rueckert, and Z. Wang, “Real-time single image and video super-resolution using an efficient sub-pixel convolutional neural network,” in *Proceedings of the IEEE conference on computer vision and pattern recognition*, 2016, pp. 1874–1883.
- [43] R. Dian and S. Li, “Hyperspectral image super-resolution via subspace-based low tensor multi-rank regularization,” *IEEE Transactions on Image Processing*, vol. 28, no. 10, pp. 5135–5146, 2019.
- [44] S. He, H. Zhou, Y. Wang, W. Cao, and Z. Han, “Super-resolution reconstruction of hyperspectral images via low rank tensor modeling and total variation regularization,” in *2016 IEEE International Geoscience and Remote Sensing Symposium (IGARSS)*. IEEE, 2016, pp. 6962–6965.
- [45] F. Yasuma, T. Mitsunaga, D. Iso, and S. K. Nayar, “Generalized assorted pixel camera: postcapture control of resolution, dynamic range, and spectrum,” *IEEE transactions on image processing*, vol. 19, no. 9, pp. 2241–2253, 2010.
- [46] A. Chakrabarti and T. Zickler, “Statistics of Real-World Hyperspectral Images,” in *Proc. IEEE Conf. on Computer Vision and Pattern Recognition (CVPR)*, 2011, pp. 193–200.
- [47] S. M. Nascimento, K. Amano, and D. H. Foster, “Spatial distributions of local illumination color in natural scenes,” *Vision research*, vol. 120, pp. 39–44, 2016.
- [48] D. P. Kingma and J. Ba, “Adam: A method for stochastic optimization,” *arXiv preprint arXiv:1412.6980*, 2014.
- [49] J. Kim, J. Kwon Lee, and K. Mu Lee, “Accurate image super-resolution using very deep convolutional networks,” in *Proceedings of the IEEE conference on computer vision and pattern recognition*, 2016, pp. 1646–1654.
- [50] Y. Zhang, K. Li, K. Li, L. Wang, B. Zhong, and Y. Fu, “Image super-resolution using very deep residual channel attention networks,” in *Proceedings of the European conference on computer vision (ECCV)*, 2018, pp. 286–301.
- [51] L. Loncan, L. B. De Almeida, J. M. Bioucas-Dias, X. Briottet, J. Chanussot, N. Dobigeon, S. Fabre, W. Liao, G. A. Licciardi, M. Simoes, *et al.*, “Hyperspectral pansharpening: A review,” *IEEE Geoscience and remote sensing magazine*, vol. 3, no. 3, pp. 27–46, 2015.
- [52] R. H. Yuhas, A. F. Goetz, and J. W. Boardman, “Discrimination among semi-arid landscape endmembers using the spectral angle mapper (sam) algorithm,” in *Proc. Summaries 3rd Annu. JPL Airborne Geosci. Workshop*, vol. 1, 1992, pp. 147–149.
- [53] L. Wald, *Data fusion: definitions and architectures: fusion of images of different spatial resolutions*. Presses des MINES, 2002.
- [54] Z. Wang, A. C. Bovik, H. R. Sheikh, and E. P. Simoncelli, “Image quality assessment: from error visibility to structural similarity,” *IEEE transactions on image processing*, vol. 13, no. 4, pp. 600–612, 2004.